frontiers in Sensors

TYPE Original Research
PUBLISHED 24 April 2026
DOI 10.3389/fsens.2026.1753123

OPEN ACCESS

EDITED BY
Lei Kou,
Qilu University of Technology (Shandong Academy of Sciences), China

REVIEWED BY
Zhengliang Zhu,
Jimei University, China
Sq Joe,
Chinese Academy of Sciences (CAS), China

*CORRESPONDENCE
Xinliang Pang,
pangxinliang@sina.com
Yunping Liu,
002105@nuist.edu.cn

†These authors have contributed equally to this work

RECEIVED 24 November 2025
REVISED 13 March 2026
ACCEPTED 25 March 2026
PUBLISHED 24 April 2026

CITATION
Li X, Song Z, Pang X, Yang F, Lu Y, Chang Y, Yin H and Liu Y (2026) Embedded very-low-frequency underwater acoustic acquisition technology and experimental study for underwater explosion monitoring.
Front. Sens. 7:1753123.
doi: 10.3389/fsens.2026.1753123

Embedded very-low-frequency underwater acoustic acquisition technology and experimental study for underwater explosion monitoring

Xuexu Li[1,2†], Zhen Song[2†], Xinliang Pang[2*], Fan Yang[2], Yu Lu[2], Yunfen Chang[2], Hao Yin[2] and Yunping Liu[1*]

[1]School of Automation, Nanjing University of Information Science and Technology, Nanjing, China, [2]State Key Laboratory of Chemistry for NBC Hazards Protection, Beijing, China

Very-low-frequency (VLF) underwater acoustic monitoring is a primary means for monitoring specialized underwater explosions. In view of the limited availability of dedicated off-the-shelf VLF underwater acoustic monitoring equipment and related technologies, this study investigates embedded VLF underwater acoustic acquisition techniques and develops an embedded acquisition device for VLF signals generated by specialized underwater explosions. The device adopts a modular architecture that separates the sensor from the controller, and integrates a low-noise transimpedance amplification and differential conditioning circuit, a high-resolution ADS1285 analog-to-digital converter, an STM32F429 control core, and an eMMC-based storage system. Multi-node time consistency is achieved through GNSS timing combined with a PPS synchronization mechanism, while cyclic recording and plug-and-play data export are implemented using the FATFS file system and USB MSC mode. In underwater explosion experiments, the device successfully recorded the initial shock-wave arrival, bubble pulsation signals, and long-range VLF underwater acoustic signals, thereby demonstrating the capability of the system for low-noise acquisition, reliable time synchronization, and long-term autonomous monitoring. The results indicate that the device can provide long-term stable acquisition and storage capabilities, meeting the engineering requirements of VLF underwater acoustic monitoring, explosion effect assessment, and underwater acoustic experiments, and offering key technical support for the development of VLF underwater acoustic monitoring equipment.

KEYWORDS
embedded acquisition device, eMMC storage, GNSS timing, underwater explosion monitoring, very-low-frequency underwater acoustic signal

1 Introduction

Underwater explosions release high-temperature and high-pressure gas within a short time, generating intense shock waves that, after long-range propagation, evolve into typical very-low-frequency (VLF) underwater acoustic signals. At ranges of hundreds of kilometers, the dominant frequency components are mostly concentrated in the tens of hertz, and at ranges of over one thousand kilometers they can be reduced to only a few hertz. Such VLF underwater acoustic signals with dominant frequencies from a few hertz to several tens of hertz exhibit long propagation distances, slow energy attenuation, and rich information content (Siyu et al., 2024; Li X. et al., 2023). These signals have important application value in explosion monitoring, yield inversion, estimation of explosion depth, and propagation environment analysis (Cole and Weller, 1948; Wang P. et al., 2023; Li M. K. et al., 2023; Huang et al., 2025). After the shock wave decays, the explosion bubble undergoes an expansion–contraction oscillation process, producing periodic bubble pulsation signals. These signals contain information on explosion loading, boundary constraints, and fluid dynamic characteristics, and thus provide an important basis for identifying the type and scale of the explosion (Dall'Osto et al., 2023; Wang Y. et al., 2024; Liu et al., 2022).

Compared with mature medium- and high-frequency underwater acoustic measurement systems, very-low-frequency underwater acoustic acquisition technology has been far less studied due to its specialized application scenarios and complex background noise environment (Perez and O'Brien, 2025; Song et al., 2024; Zhufeng et al., 2022). Existing acoustic buoys and monitoring platforms are mostly optimized for the kHz–MHz bands (Wang R. et al., 2023), and it is difficult for them to maintain sufficient sensitivity and dynamic range in the VLF band (Wang M. et al., 2023; Han et al., 2024; Demeng et al., 2023; Zhao et al., 2024). In addition, VLF signals are of small amplitude and are easily affected by sea-state disturbances and background noise, so the acquisition system must feature high common-mode rejection and low-noise performance (Ruan et al., 2023; Kim et al., 2024). Studies have shown that employing a signal conditioning architecture with a JFET input stage can effectively increase the input impedance and suppress the influence of bias current on weak signals (Ru et al., 2019). High-precision Σ-Δ ADCs, owing to their excellent noise performance and dynamic range, have gradually become the mainstream choice in nuclear electronics and precision measurement fields (Tu, 2024). On the other hand, long-term observation requires devices to exhibit low power consumption, strong environmental adaptability, and high timing consistency (Tian et al., 2020; Wang X. et al., 2024). It is noteworthy that several countries have established dedicated underwater explosion monitoring networks and stations (Matsumoto et al., 2023; Ingale et al., 2025), which possess long-term monitoring and analysis capabilities for VLF explosion signals (Lavayssière et al., 2024).

However, dedicated acquisition systems specifically designed for very-low-frequency underwater explosion monitoring remain relatively limited, particularly for long-term autonomous deployments that require low-noise sensing, high dynamic range, and reliable time synchronization. Underwater explosion signals typically consist of a strong transient shock wave followed by a sequence of low-frequency bubble pulsations. These signals exhibit large dynamic range, rapid initial pressure rise, and dominant spectral components in the very-low-frequency band. Therefore, acquisition systems intended for explosion monitoring must simultaneously support low-noise sensing for weak long-range signals and sufficient dynamic range to capture high-amplitude transient events. In addition, many existing underwater acoustic monitoring platforms rely on real-time triggered acquisition or cable-based transmission architectures. Although such systems are suitable for short-term experiments or shore-based monitoring, they are less suitable for long-term autonomous underwater deployment in very-low-frequency monitoring scenarios. In contrast, the system proposed in this work is designed to support continuous autonomous acquisition, GNSS-based time synchronization, and onboard large-capacity storage, enabling long-duration monitoring of VLF underwater explosion signals.

In view of the above technical challenges in very-low-frequency underwater acoustic signal acquisition, this work develops an embedded VLF hydroacoustic acquisition device designed for autonomous underwater deployment and long-duration monitoring. The proposed system integrates a low-noise analog front-end, high-resolution Σ-Δ analog-to-digital conversion, GNSS-based timing synchronization, and reliable large-capacity onboard storage.

Compared with conventional underwater acoustic acquisition platforms that often rely on real-time triggered acquisition or cable-based transmission, the proposed device supports continuous autonomous data acquisition and onboard storage, which is particularly suitable for long-term monitoring of VLF underwater explosion signals.

The main contributions of this work can be summarized as follows.

1. A modular embedded architecture for very-low-frequency underwater acoustic acquisition is designed, integrating a low-noise transimpedance front-end, high-resolution Σ-Δ analog-to-digital conversion, and GNSS-based timing synchronization to support high-precision long-duration monitoring of weak VLF hydroacoustic signals.
2. A high-precision timing synchronization mechanism based on GNSS and PPS signals is implemented to ensure consistent time references across multiple acquisition nodes. The accuracy of the recorded signals is further verified through the bubble pulsation period extracted from underwater explosion experiments, which shows good agreement with theoretical predictions.
3. A reliable long-term data acquisition and storage framework based on industrial-grade eMMC memory and FATFS file management is developed, enabling continuous autonomous recording and convenient plug-and-play data export. Compared with conventional SD-card-based systems that require device disassembly for data retrieval, the proposed architecture significantly improves data reliability and operational efficiency during field experiments.

2 Hardware design

The hardware system adopts a modular embedded architecture consisting of a sensor front end, analog signal conditioning, high-precision analog-to-digital conversion, main control system, timing and synchronization, data storage, and external interface modules. It is designed to achieve low-noise, high-dynamic-range signal acquisition and reliable data storage.

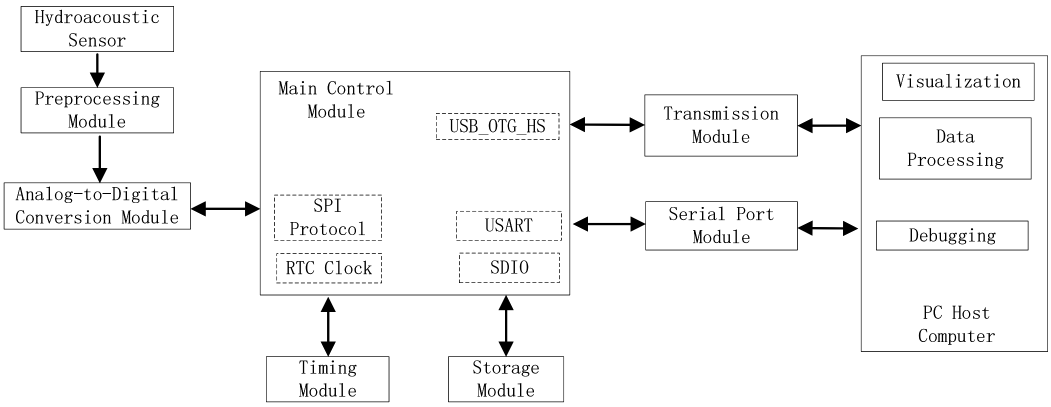

FIGURE 1
Overall hardware architecture of the device.

TABLE 1 Key specifications of the VLF underwater acoustic acquisition system.

Parameter	Specification
Hydrophone type	Self-developed spherical piezoelectric hydrophone
Hydrophone sensitivity	−193 dB re 1 V/μPa
Hydrophone operating bandwidth	1–1000 Hz
Maximum operating depth	3000 m
ADC model	ADS1285
ADC resolution	32-bit
Sampling rate	2000 Hz
Digital filter	FIR filter
Low-frequency response	DC
Transimpedance feedback resistance	10 kΩ/1 MΩ selectable
Transimpedance gain	10^4–10^6 V/A
Instrumentation amplifier gain (AD8220)	1
Electrical dynamic range	≈72 dB (raw-noise referenced)
Timing synchronization	GNSS PPS
Storage medium	eMMC

2.1 Overall architecture

The overall structure of the device is shown in Figure 1. Its core components include: the sensor module, signal conditioning and analog-to-digital conversion circuitry, an STM32F429 embedded main control unit, a GNSS timing module, a real-time clock (RTC), a large-capacity eMMC memory device, a USB communication interface, a power management and protection circuit, and a protective enclosure.

The spherical piezoelectric hydrophone employed in this work was designed for very-low-frequency underwater acoustic signal detection in deep-water environments, providing high sensitivity and stable low-frequency response required for long-range explosion signal monitoring.

To further clarify the system-level performance characteristics, the main specifications of the acquisition device are summarized in Table 1.

These specifications indicate that the system is capable of capturing both strong transient shock-wave signals and weak long-distance VLF acoustic signals generated aby underwater explosions.

2.2 Analog front-end and signal conditioning circuit

For the weak signals generated by the hydrophone sensor, the analog front-end adopts a signal-conditioning chain centered on the AD8220 instrumentation amplifier. In the present design, the AD8220 is configured at unity gain and is mainly used as a high-input-impedance buffer and signal-conditioning stage, rather than as the primary gain element. This configuration helps preserve the integrity of weak hydroacoustic signals after current-to-voltage conversion and provides a stable voltage signal for subsequent processing.

To provide a stable bias return path for the sensor, a high-value resistor is introduced at the amplifier input. Together with the sensor output, this resistor participates in the current-to-voltage conversion of the hydrophone signal, converting the sensor current into a voltage signal suitable for subsequent conditioning. Therefore, it does not represent the intrinsic input impedance of the amplifier. The effective input impedance of the front-end is mainly determined by the AD8220 itself. According to the datasheet, the input impedance of the AD8220 is approximately 10 GΩ, with an input capacitance of about 5 pF. This value is several orders of magnitude higher than the 1 MΩ resistor used in the input stage, indicating that the resistor mainly provides bias stabilization and current-to-voltage conversion rather than limiting the effective input impedance of the front-end.

The signal successively passes through transimpedance amplification, voltage scaling, and single-ended-to-differential

 10.3389/fsens.2026.1753123

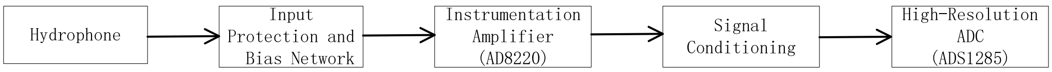

FIGURE 2
Functional block diagram of the signal conditioning chain.

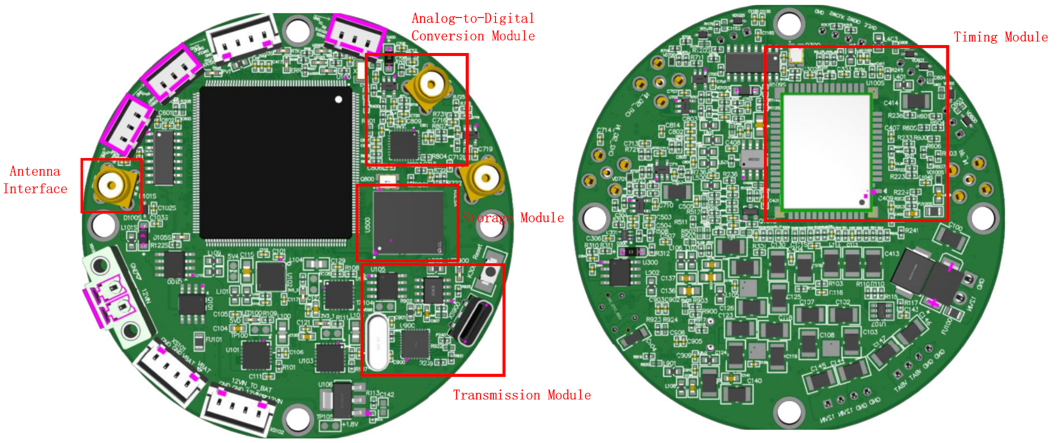

FIGURE 3
Layout of the main hardware functional modules.

conversion, and is finally converted into a ± 2.5 V differential voltage that matches the input range of the ADS1285.

Although the hydrophone output is single-ended, the ADS1285 employs a differential input structure. Therefore, the signal-conditioning stage converts the sensor output into a differential signal before ADC sampling. This differential architecture improves common-mode interference rejection and signal integrity, which is particularly important for very-low-frequency weak-signal acquisition in underwater environments.

This signal-conditioning architecture provides sufficient input-range flexibility for underwater explosion signal acquisition, enabling the circuit to accommodate both stronger transient responses and weaker very-low-frequency components without front-end saturation under appropriate configuration. This capability supports reliable recording of the main transient shock-wave response and the subsequent bubble pulsation signals associated with underwater explosions.

To further characterize the low-noise performance of the proposed acquisition system, the background noise level was estimated from the first half of a signal segment acquired under static test conditions without explosion events. The measured voltage noise is approximately 431 μV RMS before filtering and 119 μV RMS after notch filtering. Using the hydrophone sensitivity of −193 dB re 1 V/μPa, the corresponding equivalent acoustic noise is approximately 1.93 Pa RMS before filtering and 0.53 Pa RMS after filtering at the system level. These results indicate that the proposed low-noise analog front-end provides sufficient sensitivity for weak very-low-frequency underwater acoustic signal acquisition.

Based on the measured system-level voltage noise and the usable input range of the analog-to-digital conversion stage, the electrical dynamic range of the acquisition chain can be estimated. Taking the measured voltage noise before filtering (431 μV RMS) as the reference noise level and considering the usable input range of the ADS1285 interface, the corresponding electrical dynamic range of the present system is approximately 72 dB. If the notch-filtered noise level (119 μV RMS) is used as the reference, the effective dynamic range can reach approximately 83 dB. In addition, two selectable transimpedance resistor configurations (10 kΩ and 1 MΩ) are provided in the analog front-end to adapt the sensitivity of the acquisition circuit to signals of different amplitudes. This configuration improves the practical dynamic-range flexibility of the system, enabling it to accommodate both weak very-low-frequency signals and stronger transient components generated by underwater explosion events.

The functional block diagram of the signal conditioning chain is shown in Figure 2.

2.3 Analog-to-digital conversion and main control system

To capture very-low-frequency weak signals, the system employs the 32-bit high-precision ADS1285 analog-to-digital converter as the core acquisition device. This chip integrates a programmable gain amplifier (PGA) and configurable digital filters, offering excellent dynamic range and low-noise performance, and is particularly suitable for long-range sensing scenarios with stringent requirements on signal integrity.

The ADS1285 is configured as the core high-resolution analog-to-digital converter in the acquisition system, with its peripheral

TABLE 2 Description of the system state machine.

State	Name	Core functions and transitions
V1	Initialization	Completes hardware and software initialization to prepare for system startup
V2	Time waiting	Listens to GNSS for accurate time; falls back to the local clock upon timeout to ensure acquisition initiation
V3	First synchronization	Parses GNSS time and uses the PPS signal to perform high-precision calibration of the RTC.
V4	Periodic resynchronization	Periodically reconnects to GNSS during the main acquisition phase to correct RTC drift
V5	Continuous acquisition	Main operating mode: performs data acquisition, buffering, and storage, while responding to USB connection events

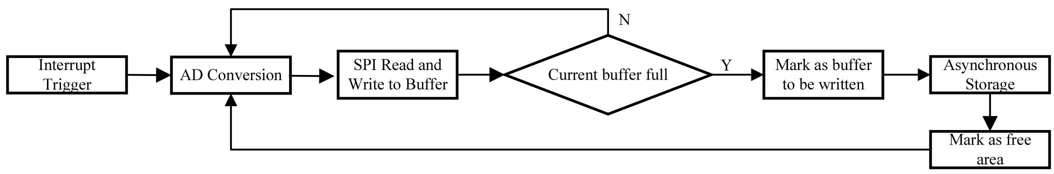

FIGURE 4
Buffer scheduling mechanism.

circuits designed according to the manufacturer's recommended configuration.

In the present configuration, the ADS1285 was operated at a data output rate of 2000 Hz with the FIR digital filter enabled. According to the filter response, the effective pass-band extends from DC to approximately $0.375f_{\mathrm{DATA}}$, corresponding to about 750 Hz.

The system's main control unit is an STM32F429 microcontroller, which initiates the sampling process of the ADS1285 and uses direct memory access (DMA) to achieve high-speed, non-blocking transfer of sampled data. This architecture effectively coordinates multi-level buffering and storage scheduling, ensuring real-time responsiveness and data integrity during continuous acquisition.

The sampling accuracy of the acquisition system is mainly determined by the stability of the master clock driving the ADS1285. In the current design, the ADC is driven by a 4.096 MHz clock source with a frequency stability of approximately ± 20 ppm. Therefore, the corresponding sampling rate deviation at 2000 SPS is within ± 0.04 Hz, ensuring stable and reliable acquisition of very-low-frequency underwater acoustic signals during long-duration monitoring.

The combination of the high-resolution Σ-Δ ADC and the low-noise analog front-end enables the system to maintain sufficient electrical dynamic range for both weak long-range VLF signals and stronger transient acoustic responses.

2.4 High-precision timing module design

In multi-node cooperative observations, a unified time reference is essential (Zhang, 2025). The device adopts a hybrid synchronization strategy combining GNSS timing and an RTC. A BeiDou-based timing module (UM980) is integrated; by parsing its output UTC time messages and using the 1 Hz PPS (pulse-per-second) signal, the internal RTC of the STM32F429 is calibrated at the hardware level. This design effectively suppresses clock drift, ensures the continuity and accuracy of data timestamps, and provides a reliable time base for joint data analysis across multiple devices.

2.5 FATFS file system and data management

Long-term continuous acquisition imposes stringent requirements on the reliability and continuity of write operations in the data storage system, while conventional SD cards exhibit limited performance in terms of power-loss protection and write stability (Bi et al., 2023; Qin et al., 2025; Thomas-Brans et al., 2024). To meet the high reliability demands of long-duration continuous acquisition, the system adopts an industrial-grade eMMC device as the primary storage medium and connects it to the main controller via an MMC 4-bit bus to increase write bandwidth.

On the software side, the FATFS file system is integrated to manage data storage. A segmented file storage and cyclic overwrite strategy is employed to avoid storage space exhaustion. In combination with a write transaction protection mechanism, this approach significantly reduces the risk of data corruption caused by unexpected power loss and achieves a balance between high throughput and data security (Kachman et al., 2025).

2.6 USB communication module and MSC mode design

To facilitate data export, the system incorporates a USB 2.0 communication module based on the USB3320 high-speed PHY chip and a USB Type-C connector. At the protocol level, the USB mass storage class (MSC) mode is implemented, allowing the device to be recognized as an external USB drive when connected to a PC.

Figure 3 shows the physical device and the layout of its main functional modules. The modules work together through standard

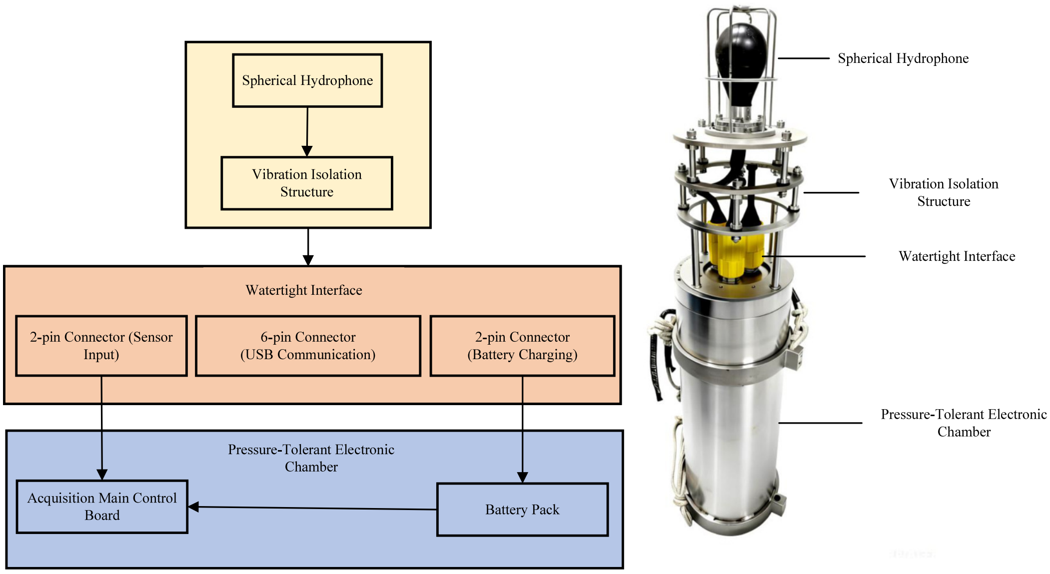

FIGURE 5
Assembled prototype of the embedded acquisition device.

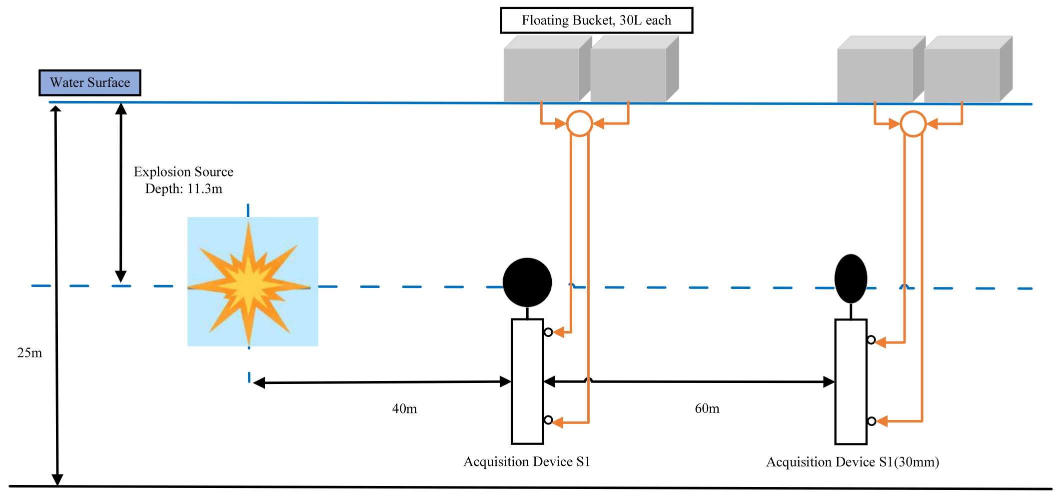

FIGURE 6
Experimental layout of the lake tests.

interfaces, providing a robust hardware foundation for subsequent software design and function implementation.

3 Software design

The embedded software of the acquisition system was developed in the C programming language on the STM32 platform. The software design follows the principles of "prioritizing acquisition continuity, data security, and time consistency," and implements an embedded acquisition architecture centered on a state machine, supporting long-term, unattended operation.

3.1 System state machine design

The system operation is governed by five core states, whose functions and transition logic are summarized in Table 2.

3.2 Acquisition and buffering mechanism

To ensure data integrity during continuous acquisition, the system implements a parallel data transfer pipeline consisting of front-end sampling, DMA transfer, multi-level buffering, and file storage.

TABLE 3 Comparison between theoretical and measured first bubble pulsation periods.

Channel	Date	Measured period (s)	Theoretical period (s)	Relative deviation (%)
S1	2025-08-19	0.437	0.4945	−11.63
S1	2025-08-20	0.472	0.4945	−4.55
S2	2025-08-19	0.484	0.4945	−2.12
S2	2025-08-20	0.472	0.4945	−4.55

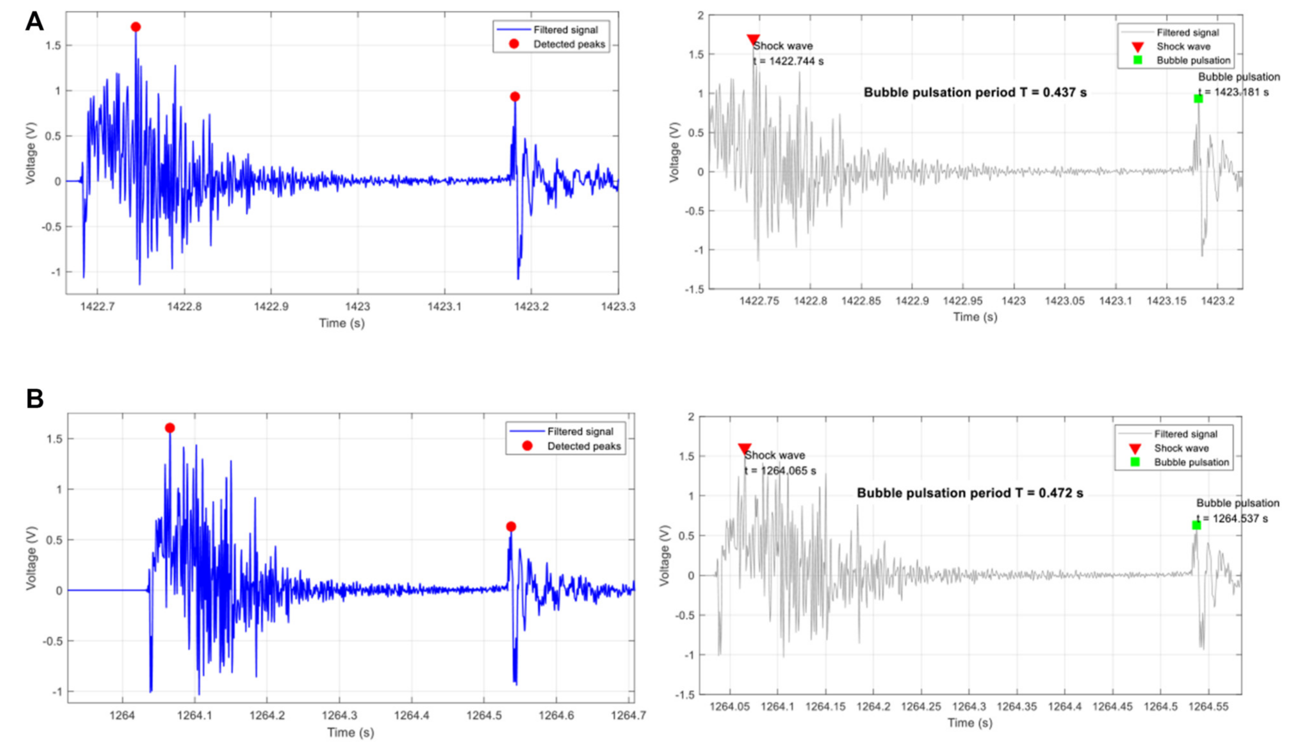

FIGURE 7
Bubble pulsation signals and extracted periods for the S1 channel in lake explosion tests. **(A)** Overall signal and detected peaks–Test 1 (2025-08-19). **(B)** Overall signal and detected peaks–Test 2 (2025-08-20).

Data flow organization: The data-ready (DRDY) signal of the ADS1285 triggers the main controller to transfer data directly into a RAM buffer via DMA, achieving non-blocking acquisition.

Buffer scheduling: As shown in Figure 4, a triple-buffer mechanism is adopted, consisting of an active buffer, a write-pending buffer, and an idle buffer. The active buffer receives data in real time; once a data block is full, it is swapped with the write-pending buffer, which is then written to eMMC asynchronously by the file system, while the idle buffer waits to be reassigned. This mechanism effectively decouples acquisition from storage and prevents data loss caused by write latency.

4 Experimental validation

To evaluate the practical performance of the system, we carried out system integration tests as well as underwater explosion lake tests and sea trials.

4.1 Prototype structure and assembly

The prototype adopts an integrated, vertically stacked configuration consisting of a spherical piezoelectric hydrophone, a vibration-isolation support, and a pressure-resistant metallic electronics housing. Inside the electronics housing, the signal-conditioning/power board, data acquisition and control board, and battery pack are arranged from top to bottom. Externally, watertight connectors are used to provide hydrophone input, battery charging, and USB communication. The assembled prototype is shown in Figure 5.

4.2 Lake test configuration and data acquisition

The lake experiments were conducted in an inland water area, with the explosive source deployed at a water depth of approximately 11.3 m. Two acquisition systems were equipped

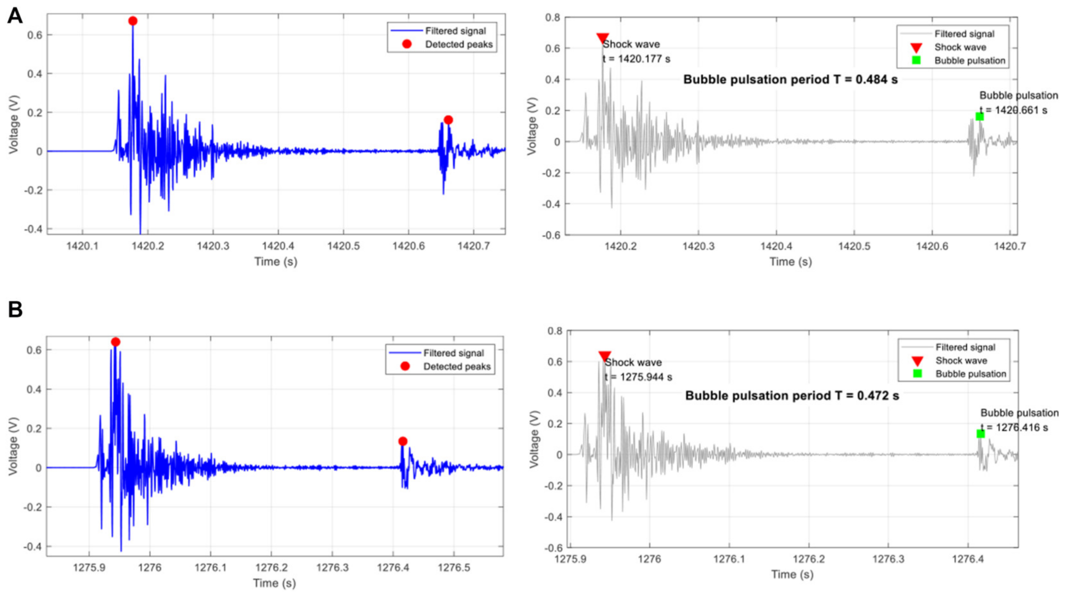

FIGURE 8
Bubble pulsation signals and extracted periods for the S2 channel in lake explosion tests. **(A)** Overall signal and detected peaks–Test 1 (2025-08-19). **(B)** Overall signal and detected peaks–Test 2 (2025-08-20).

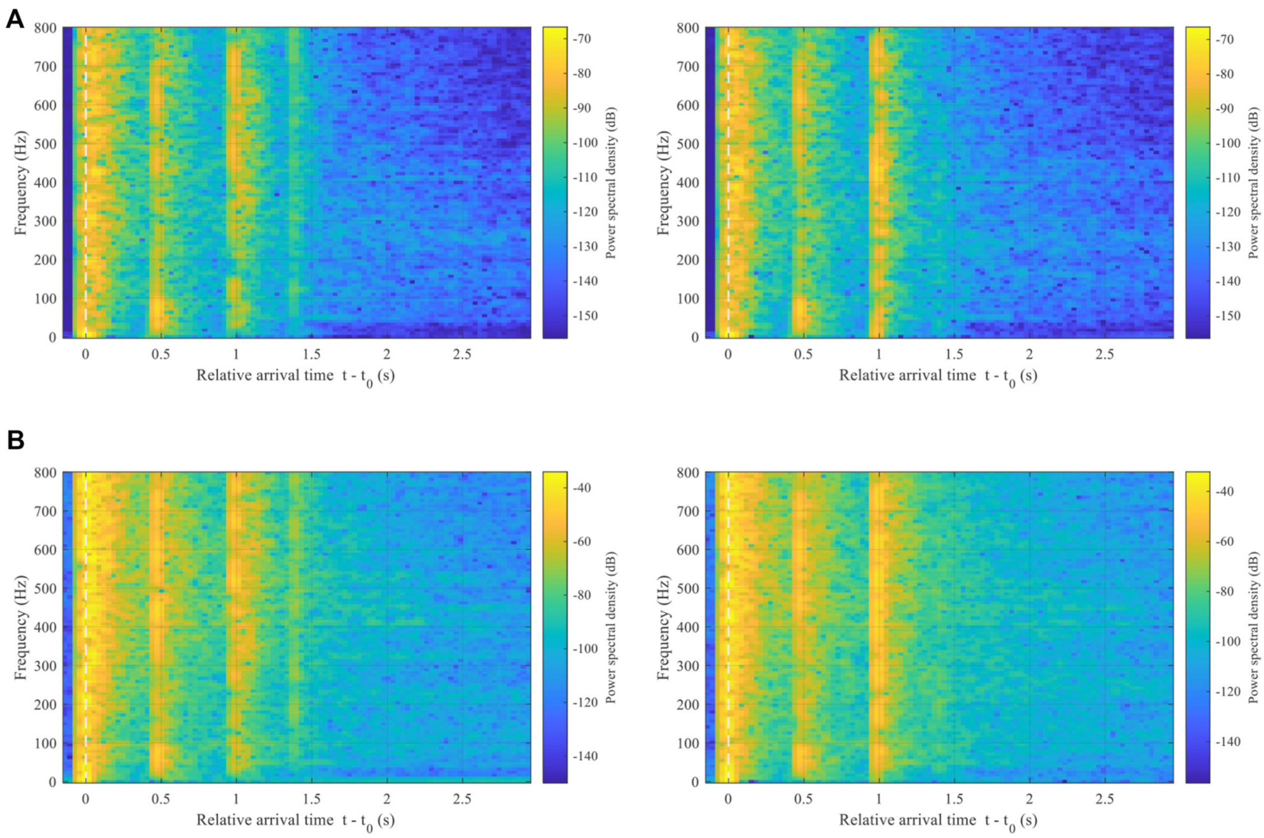

FIGURE 9
STFT spectrograms of underwater explosion signals recorded during the lake tests. **(A)** S1-Test1 and S1-Test2. **(B)** S2-Test1 and S2-Test2. The vertical dashed line denotes the detected first arrival time t_0. The subsequent high-energy bands represent the bubble pulsation sequence generated by the underwater explosion.

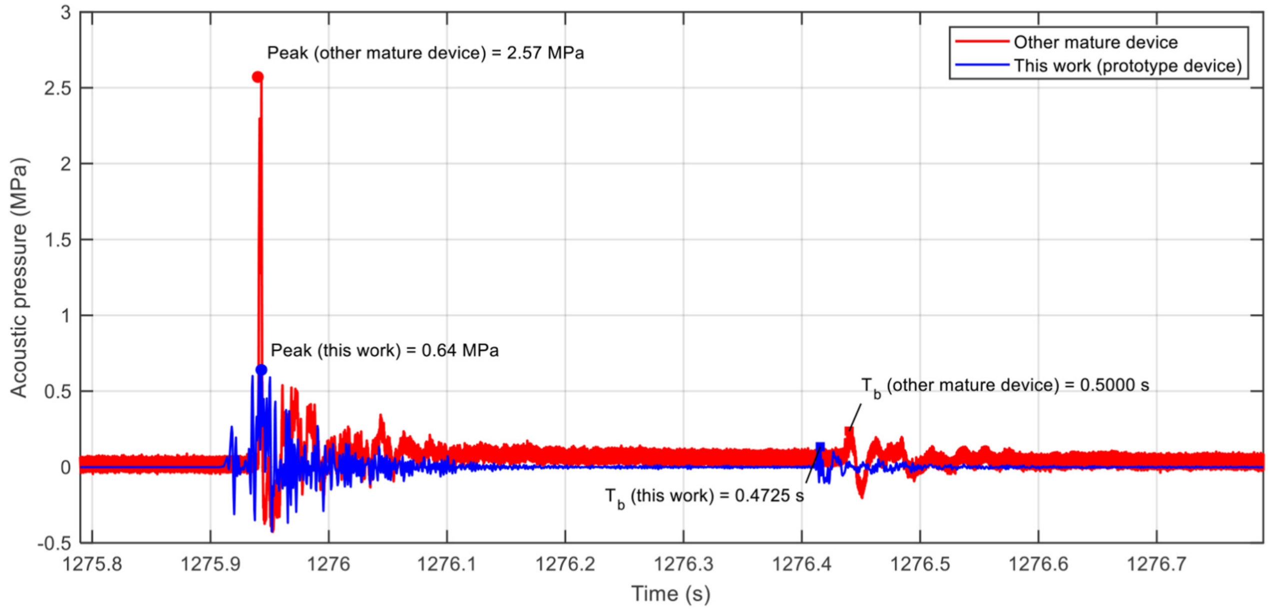

FIGURE 10
Comparison of time-domain signals recorded by the prototype hydrophone system and a reference hydrophone at a horizontal distance of 40 m from the explosion source.

with S1 and S2 sensors, respectively, and were deployed in the same direction relative to the source, with horizontal offsets of about 40 m and 100 m. The systems were suspended and positioned using floats, and the deployment depth of the acquisition devices was kept consistent with the hydrophone depth. The experimental configuration is illustrated in Figure 6.

4.3 Experimental results and analysis

To verify the capability of the system to capture underwater explosion signals and to assess the validity of the acquired data, two sets of field experimental data were analyzed. All recordings clearly contain the initial shock-wave response and the subsequent bubble pulsation sequence, indicating that the system is capable of reliably capturing the main acoustic features of the underwater explosion process.

4.3.1 Verification of numerical validity

The bubble pulsation period of an underwater explosion is a key parameter reflecting the explosion yield and energy conversion (Li Y. F. et al., 2023). A shallow-water corrected model developed on the basis of Cole's classical theory is widely used in bubble dynamics analysis (Xie and Sun, 2024; Zhou et al., 2024), and the period of the first pulsation can be expressed by Equation 1:

$$T = 2.11W^{1/3} \Big/ (H + 10.3)^{5/6} \qquad (1)$$

where T is the first bubble pulse period (s), W is the explosive yield (kg TNT equivalent), and H is the depth of the explosive source (m).

The bubble pulsation periods extracted from the measured signals are summarized in Table 3. The corresponding analysis results are presented in Figures 7, 8, where the upper panels show the filtered signals and the lower panels highlight the bubble pulsation segments.

As shown in Figure 7, Channel S1 clearly records the initial shock-wave response and the subsequent multi-cycle bubble pulsation sequence for both tests. The extracted first bubble pulsation periods agree well with the theoretical values derived from the shallow-water-corrected Cole model.

Under the same explosive yield and deployment geometry, the signals recorded by Channel S2 are generally consistent with those of Channel S1, but exhibit a higher signal-to-noise ratio (SNR) in the bubble pulsation segment. This facilitates more reliable period identification, and the corresponding processing results are presented in Figure 8.

The time–frequency characteristics of the recorded explosion signals are further illustrated in Figure 9. The spectrograms clearly reveal the initial shock wave followed by multiple bubble pulsation cycles, with energy mainly distributed below 800 Hz.

4.3.2 Comparison with a reference hydrophone

To further evaluate the measurement reliability of the developed acquisition system, a comparative experiment was conducted using a reference hydrophone measurement system deployed under the same experimental conditions. Both hydrophones recorded the acoustic signals generated by the same underwater explosion event.

Figure 10 presents the time-domain signals recorded by the two systems. The reference hydrophone captured a peak pressure of approximately 2.57 MPa, whereas the prototype acquisition system recorded a peak value of about 0.64 MPa. This difference is mainly attributed to the sampling configuration of the prototype system. In order to support long-duration continuous monitoring of very-low-frequency underwater acoustic signals, the sampling rate of the

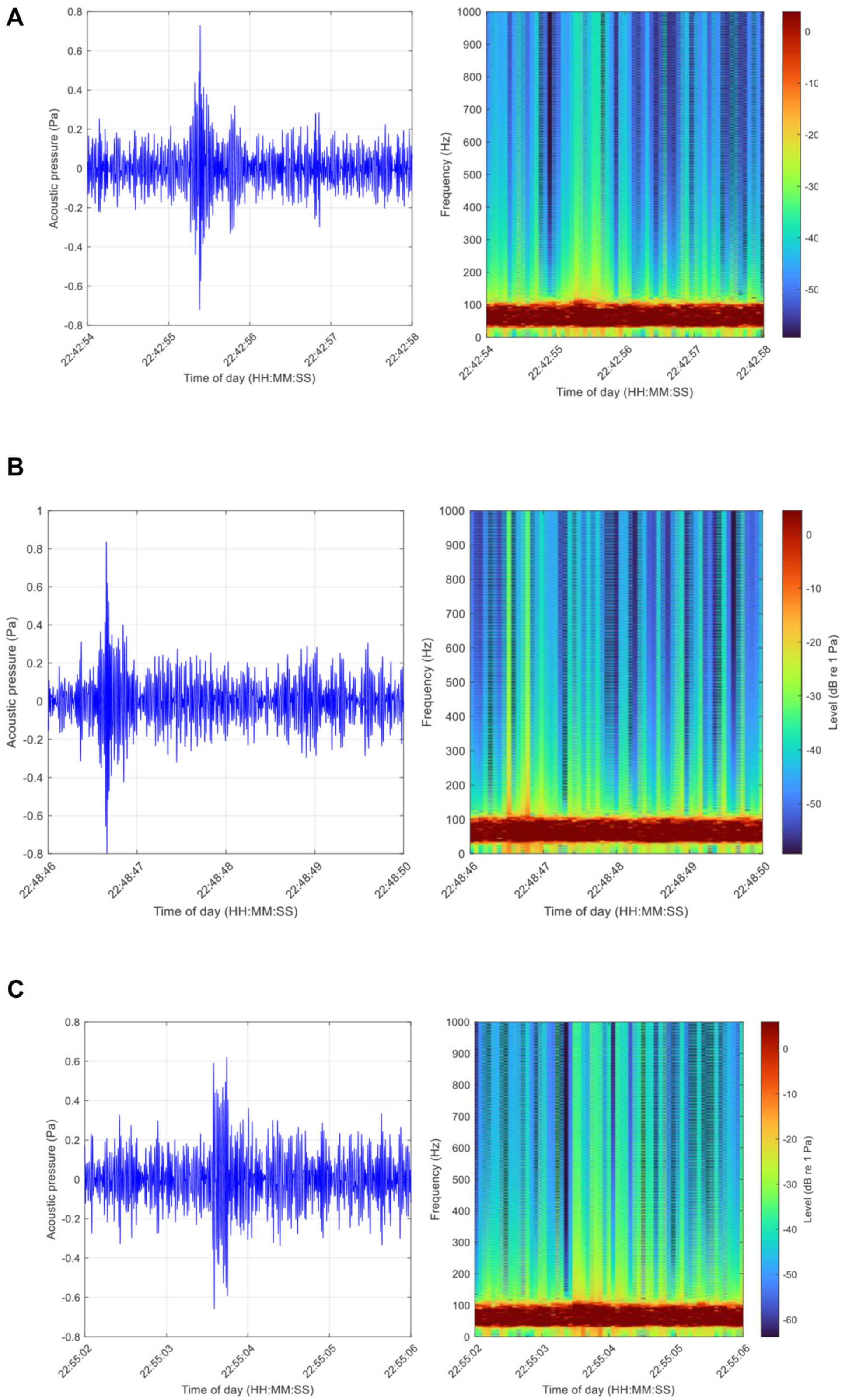

FIGURE 11
Acoustic pressure waveforms and spectrograms of three underwater explosion shots. **(A)** Acoustic pressure waveform and spectrogram of Shot 1. **(B)** Acoustic pressure waveform and spectrogram of Shot 2. **(C)** Acoustic pressure waveform and spectrogram of Shot 3.

TABLE 4 Explosion source information and time–frequency characteristics of three representative 1 kg TNT-equivalent events recorded by the developed system at an explosion depth of 300 m.

Shot no.	Equivalent–Depth	Range/km	Pressure amplitude/Pa	Dominant frequency/Hz
1	1 kg–300 m	522.6	0.82	75
2	1 kg–300 m	521.9	0.94	75
3	1 kg–300 m	521.1	0.70	55

device was configured as 2000 Hz, which may limit the ability to fully resolve the millisecond-scale peak pressure of the explosion shock wave.

Despite this difference in peak amplitude, the overall waveform structures recorded by the two systems exhibit strong similarity. In particular, the bubble pulsation signals following the initial shock wave can be clearly identified in both recordings. The first bubble pulsation periods extracted from the two datasets are approximately 0.50 s for the reference hydrophone and 0.48 s for the prototype system. These values are consistent with the theoretical first bubble pulsation period of approximately 0.49 s predicted by the shallow-water corrected Cole model (Table 3).

Overall, the comparison indicates that although the prototype system is optimized for continuous very-low-frequency monitoring rather than high-speed transient capture, it can reliably record the main temporal characteristics of underwater explosion signals. In particular, the bubble pulsation features, which are closely related to explosion yield and depth, are clearly reproduced in the recordings of the developed system.

4.3.3 Verification in an open-sea environment

Acquisition units were deployed in the far field at ranges of 518–523 km. In the following analysis, three representative signals recorded by the developed system for 1 kg TNT-equivalent explosion events at a depth of 300 m are first presented. Subsequently, comparison results between the developed system and a reference hydrophone are provided for three representative events with explosion depths of 300 m, 100 m, and 1000 m.

Taking the 1 kg TNT-equivalent explosion events at a depth of 300 m as representative examples, the corresponding waveforms and spectra recorded by the developed system are shown in Figure 11. The analysis indicates that the device can clearly record and effectively distinguish different explosion events. As summarized in Table 4, at propagation distances exceeding 520 km, the system can still reliably capture VLF signals with amplitudes of 0.70–0.94 Pa and dominant frequencies concentrated in the 55–75 Hz band. These results demonstrate the effectiveness of the device for long-range detection of underwater explosion signals in real ocean conditions.

To further assess the reliability of the proposed acquisition system beyond the 300 m representative cases presented above, additional comparisons were carried out using signals recorded simultaneously by a reference hydrophone during the same sea trial. Three representative explosion events with depths of 300 m, 100 m, and 1000 m were selected for comparison.

The corresponding waveform and spectrogram comparisons between the reference hydrophone and the proposed system are shown in Figures 12, 13.

As illustrated in Figures 12, 13, the two systems exhibit consistent temporal structures for all three explosion events. The developed acquisition system clearly captures the transient waveform characteristics associated with the explosion signals, and the main energy bursts occur within similar time intervals as those recorded by the reference hydrophone. Although differences in absolute amplitude can be observed due to variations in sensor sensitivity, installation configuration, and signal processing procedures, the overall waveform envelopes remain comparable.

The spectrogram comparison further demonstrates that the dominant spectral components recorded by the proposed system are highly consistent with those observed by the reference hydrophone. In particular, the main acoustic energy is concentrated in the low-frequency band, while the dominant peak frequencies of the representative events fall within approximately 55–75 Hz, which agrees with the typical spectral characteristics of long-range underwater explosion signals.

Quantitative comparison results are summarized in Table 5. The peak acoustic pressures measured by the developed hydrophone for the three events are approximately 0.73 Pa, 0.39 Pa, and 0.37 Pa, respectively, while the corresponding root-mean-square (RMS) pressures range from 0.09 to 0.11 Pa.

The recorded signal amplitudes in the open-sea experiments (0.70–0.94 Pa) are higher than the estimated system-level noise floor, confirming that the proposed acquisition system provides sufficient sensitivity for long-range VLF underwater explosion monitoring.

Despite the amplitude differences between the two systems, the dominant frequencies detected by the proposed system remain stable within the low-frequency band, and the waveform correlation coefficients indicate consistent signal characteristics between the recordings.

These observations confirm that the proposed hydrophone acquisition system can reliably reproduce the key temporal and spectral features of underwater explosion signals detected by the reference hydrophone. The results further demonstrate the effectiveness and robustness of the proposed system for long-range underwater acoustic monitoring in deep-sea environments.

5 Conclusion

In response to the urgent demand for very low frequency (VLF) hydroacoustic signal acquisition in specialized underwater explosion monitoring, and the limitations of existing equipment

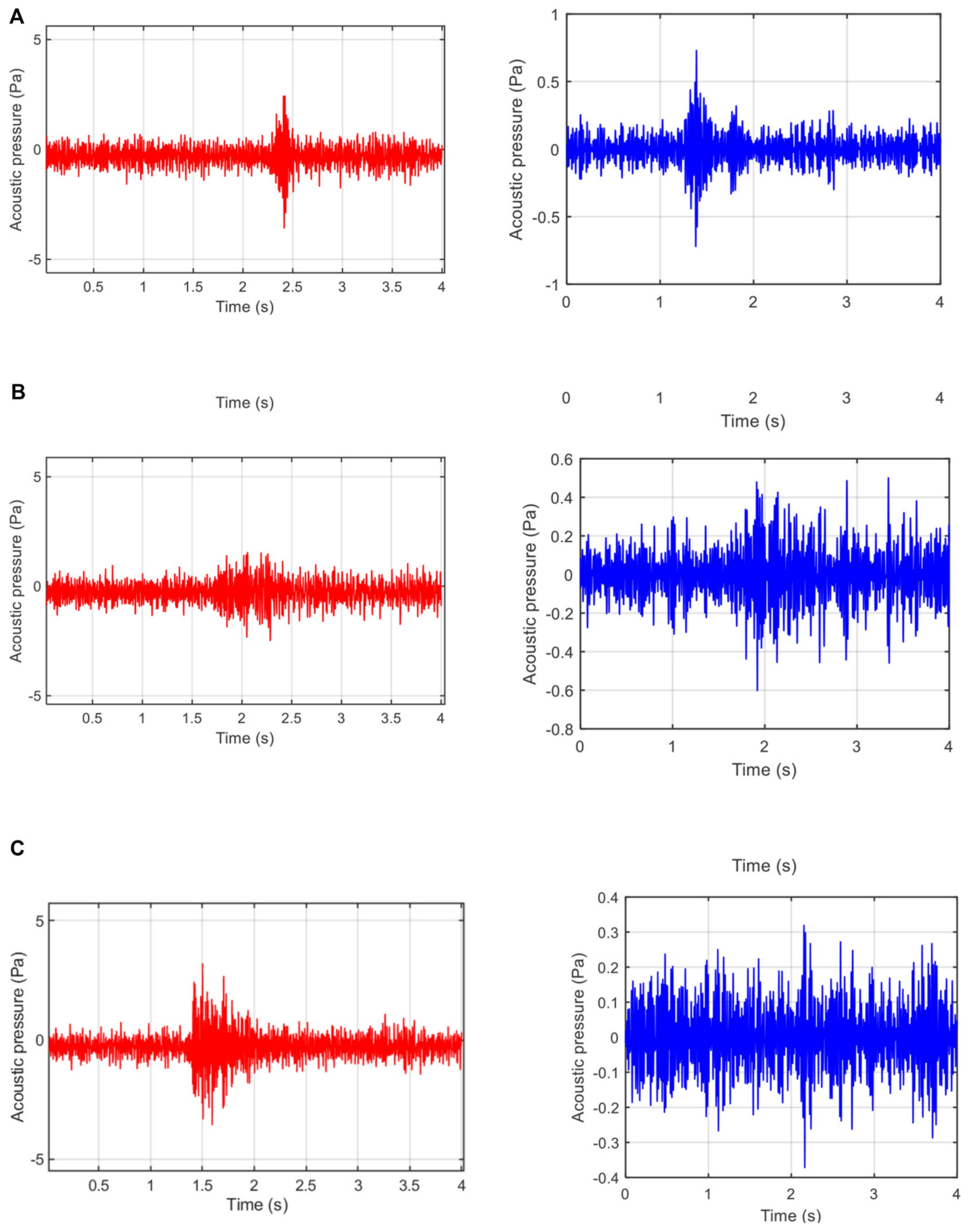

FIGURE 12
Waveform comparisons between the reference hydrophone and the developed hydrophone for three underwater explosion events. In each panel, the left subplot shows the reference hydrophone result and the right subplot shows the developed hydrophone result. **(A)** Waveform comparison for the 1 kg × 300 m explosion event at 522.6 km **(B)** Waveform comparison for the 1 kg × 100 m explosion event at 519.5 km. **(C)** Waveform comparison for the 1 kg × 1000 m explosion event at 518.4 km.

in low-frequency response, time synchronization, and long-term deployment, this study developed an embedded VLF hydroacoustic acquisition system. Its performance was evaluated through lake and sea trials. The main conclusions are as follows.

1. The developed acquisition device integrates a low-noise analog front end, a high-resolution analog-to-digital converter (ADC), a high-precision GNSS timing module, and a large-capacity eMMC storage system. It exhibits low noise, adequate electrical dynamic range, and high temporal consistency, enabling effective recording of the main transient shock-wave response, bubble pulsation signals, and distant VLF hydroacoustic signals.
2. By incorporating the FATFS file system and a triple-buffering mechanism, continuous data acquisition and highly reliable

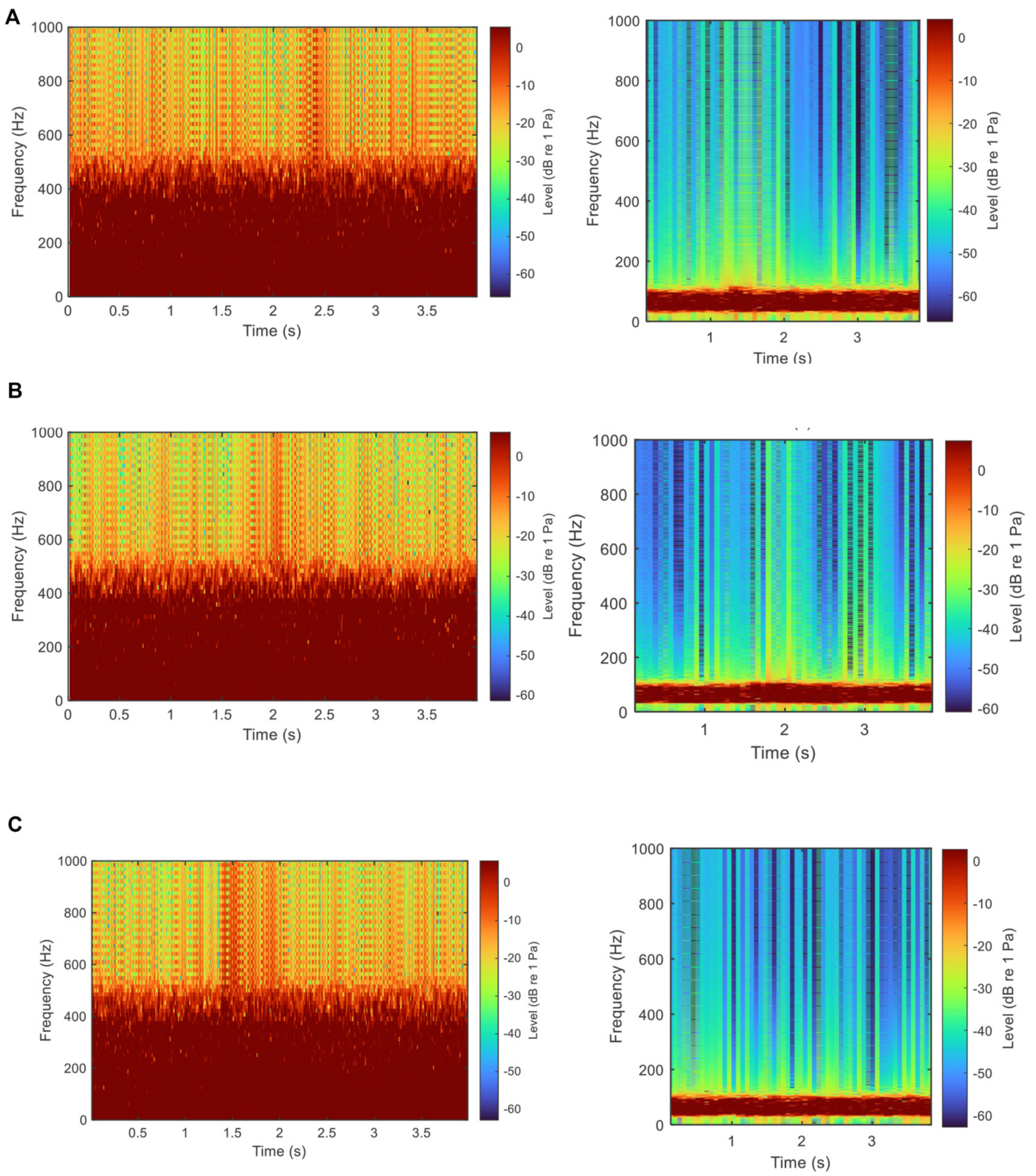

FIGURE 13
Spectrogram comparisons between the reference hydrophone and the developed hydrophone for three underwater explosion events. In each panel, the left subplot shows the reference hydrophone result and the right subplot shows the developed hydrophone result. **(A)** Spectrogram comparison for the 1 kg × 300 m explosion event at 522.6 km **(B)** Spectrogram comparison for the 1 kg × 100 m explosion event at 519.5 km **(C)** Spectrogram comparison for the 1 kg × 1000 m explosion event at 518.4 km.

TABLE 5 **Quantitative comparison between the reference hydrophone and the proposed system.**

Event	Equivalent–Depth	Ref. Peak/Pa	Dev. Peak/Pa	Ref. RMS/Pa	Dev. RMS/Pa
Event 1	1 kg–300 m	5.66	0.73	0.57	0.11
Event 2	1 kg–100 m	5.68	0.39	0.57	0.11
Event 3	1 kg–1000 m	5.67	0.37	0.61	0.09

storage were achieved. The plug-and-play data export feature based on the USB mass storage class (MSC) protocol significantly improves system maintainability and field data processing efficiency, meeting the requirements for long-term unattended operation.
3. Lake and sea trial results demonstrate that the system is capable of recording the main acoustic features of underwater explosions, including the main shock-wave response and bubble pulsation signals. The extracted bubble pulsation periods show good agreement with classical theoretical models, with a maximum relative deviation of less than 11.63%.
4. The proposed embedded acquisition system provides a practical technical approach for VLF hydroacoustic signal acquisition in underwater explosion monitoring.

Data availability statement

The raw data supporting the conclusions of this article will be made available by the authors, without undue reservation.

Author contributions

XL: Conceptualization, Methodology, Software, Validation, Investigation, Data curation, Writing – original draft, Visualization. ZS: Methodology, Software, Validation, Investigation, Data curation, Writing – review and editing. XP: Conceptualization, Resources, Supervision, Writing – review and editing, Project administration, Funding acquisition. FY: Investigation, Data curation, Validation, Visualization. YfL: Investigation, Resources, Visualization. YC: Methodology, Validation, Writing – review and editing. HY: Investigation, Resources, Software. YpL: Conceptualization, Supervision, Writing – review and editing, Project administration.

Funding

The author(s) declared that financial support was not received for this work and/or its publication.

Conflict of interest

The author(s) declared that this work was conducted in the absence of any commercial or financial relationships that could be construed as a potential conflict of interest.

Generative AI statement

The author(s) declared that generative AI was not used in the creation of this manuscript.

Any alternative text (alt text) provided alongside figures in this article has been generated by Frontiers with the support of artificial intelligence and reasonable efforts have been made to ensure accuracy, including review by the authors wherever possible. If you identify any issues, please contact us.

Publisher's note

References

Bi, R., Cui, J., Li, L., Wang, B., Yu, J., Mu, J., et al. (2023). Embedded cyclic storage technology for vehicle-mounted vibration testing based on emmc. *Foreign Electron. Meas. Technol.* 42, 113–119.

Cole, R. H., and Weller, R. (1948). Underwater explosions. *Phys. Today* 1, 35. doi:10.1063/1.3066176

Dall'Osto, D. R., Dahl, P. H., and Chapman, N. R. (2023). The sound from underwater explosions. *Acoust. Today* 19, 12–19. doi:10.1121/at.2023.19.1.12

Demeng, L., Haidong, X., Changqing, H., and Dongfei, S. (2023). A design of signal acquisition circuit for self-contained hydrophone. *Tech. Acoust.* 42, 306–313. doi:10.16300/j.cnki.1000-3630.2023.03.006

Han, W., Hu, Y., Shi, M., Lin, X., and Zou, P. (2024). "Design of high precision data acquisition system based on fpga," in *2024 5th international conference on artificial intelligence and electromechanical automation (AIEA)*. IEEE, 62–66.

Huang, X., Shang, W., Han, L., Greenhalgh, S., and Lin, J. (2025). Emitting and controlling ultra-low frequency underwater acoustic waves using a marine vibration system with time interfacing. *Commun. Eng.* 4, 51. doi:10.1038/s44172-025-00389-3

Ingale, V. V., Parnell-Turner, R., Fan, W., Talling, P. J., and Neasham, J. (2025). Hydroacoustic signals recorded by ctbto network suggest a possible submarine landslide in trou sans fond canyon, offshore Ivory coast, march 2024. *Seismol. Res. Lett.* 96, 2253–2263. doi:10.1785/0220240448

Kachman, O., Malík, P., Baláž, M., Majer, L., and Gyepes, G. (2025). A lightweight and configurable flash filesystem for low-power devices. *J. Low Power Electron. Appl.* 15, 22. doi:10.3390/jlpea15020022

Kim, G., Kim, D., and Roh, Y. (2024). Design of wideband flextensional hydrophone. *Sensors* 24, 4941. doi:10.3390/s24154941

Lavayssière, A., Bazin, S., and Royer, J. Y. (2024). Hydroacoustic monitoring of Mayotte submarine volcano during its eruptive phase. *Geosciences* 14, 170. doi:10.3390/geosciences14060170

Li, X., Chen, H., Lu, H., Bi, X., and Mo, Y. (2023a). A method of underwater sound source range estimation without prior knowledge based on single sensor in shallow water. *Front. Phys.* 11, 1109220. doi:10.3389/fphy.2023.1109220

Li, M. K., Wang, S. P., Zhang, S., and Sagar, H. (2023b). Experimental study of underwater explosions below a free surface: bubble dynamics and pressure wave emission. *Phys. Fluids* 35, 083313. doi:10.1063/5.0155177

Li, Y. F., Zhang, Y. O., Qu, Y., and Zhang, T. (2023c). A numerical approach for acoustic radiation and scattering of moving bubbles at low frequencies. *Front. Phys.* 11, 1191160. doi:10.3389/fphy.2023.1191160

Liu, J., Liu, M., Sun, C., Lin, Z., Feng, Z., Si, S., et al. (2022). Triboelectric hydrophone for underwater detection of low-frequency sounds. *Nano Energy* 99, 107428. doi:10.1016/j.nanoen.2022.107428

Matsumoto, H., Zampolli, M., Haralabus, G., Stanley, J., Robertson, J., and Özel, N. M. (2023). Hydroacoustic signals originating from marine volcanic activity at kadovar island, Papua New Guinea, recorded by the comprehensive nuclear-test-ban treaty international monitoring system. *Pure Appl. Geophys.* 180, 1353–1373. doi:10.1007/s00024-022-03096-8

Perez, T. M., and O'Brien, J. (2025). Underwater noise levels in the strait of Gibraltar and surrounding waters: findings from the amigos survey. *Front. Mar. Sci.* 12, 1655366. doi:10.3389/fmars.2025.1655366

Qin, Z., Lu, J., Men, B., Wei, S., and Pan, J. (2025). Design of a multi-node data acquisition system for logging-while-drilling acoustic logging instruments based on fpga. *Sensors Basel, Switz.* 25, 808. doi:10.3390/s25030808

Ru, H., Guo, S., and Wang, Y. (2019). Design of very low frequency piezoelectric hydrophone based on ultra low noise jfet. *Chin. J. Sens. Actuators* 32, 1775–1783.

Ruan, C., Chen, M., Yu, Y., Zhang, Y., Wang, J., Zhang, Z., et al. (2023). Research on very-low-frequency hydroacoustic acoustic velocity sensor based on dfb fiber laser. *Photonics (MDPI)* 10, 463. doi:10.3390/photonics10040463

Siyu, M., Yuxiang, Z., Zhinan, X., and Jingwei, Y. (2024). Study of very-low-frequency sound propagation characteristics in the complex ocean space based on the spectral element method. *ACTA ACUST.* 49, 844–854. doi:10.12395/0371-0025.2023045

Song, Z., Lu, Y., Pang, X., Yin, H., Chang, Y., and Shu, H. (2024). "Design and simulation of a low-frequency piezoelectric spherical hydrophone," in *2024 OES China Ocean Acoustics (COA)*. IEEE, 1–6.

Thomas-Brans, F., Fukami, A., Clement, Q., Heckmann, T., and Sauveron, D. (2024). Case of study for *in situ* memory reading on damaged multimedia card. *Forensic Sci. Int. Digital Investigation* 48, 301698. doi:10.1016/j.fsidi.2024.301698

Tian, R., Zhang, J., Zhang, S., Wang, L., Yang, H., Chen, Y., et al. (2020). A high-precision energy-efficient gps time-sync method for high-density seismic surveys. *Appl. Sci.* 10, 3768. doi:10.3390/app10113768

Tu, X. (2024). Design and implementation of an arrayed airborne nuclear radiation detection system based on sipm readout. *Nucl. Electron. and Detect. Technol.* 44, 999–1007.

Wang, P., Shi, D., Cui, X., Ma, C., Su, B., and Li, G. (2023a). Study on bubble pulsation process of underwater explosion between parallel plates with various distances. *Ocean. Eng.* 278, 114512. doi:10.1016/j.oceaneng.2023.114512

Wang, R., Zhou, Y., Yang, X., Tong, F., and Wu, J. (2023b). Design and implementation of a multi-function hydrophone for underwater acoustic application. *J. Mar. Sci. Eng.* 11, 2203. doi:10.3390/jmse11112203

Wang, M., Yi, K., and Zhu, R. (2023c). Tunable underwater low-frequency sound absorption *via* locally resonant piezoelectric metamaterials. *J. Sound Vib.* 548, 117514. doi:10.1016/j.jsv.2022.117514

Wang, Y., Tang, W., Liu, Z., Li, J., Wang, X., and Zou, S. (2024a). Analysis of nuclear explosion detection capability of ims hydroacoustic network. *Shock Vib.* 2024, 2499939. doi:10.1155/2024/2499939

Wang, X., Su, Y., and Fan, R. (2024b). Sfdm: a time-synchronization-free detection mechanism for mobile underwater acoustic sensor networks. *Ocean. Eng.* 311, 118983. doi:10.1016/j.oceaneng.2024.118983

Xie, Y., and Sun, Y. (2024). Coupling shape and load distribution characteristics of underwater explosion multi-bubble. *J. Ordnance Equip. Eng.* 45, 10–18.

Zhang, X. (2025). Design and implementation of a time synchronization system based on the beidou navigation satellite system. *Internet Things Technol.* 15, 149–152.

Zhao, J., Hu, Q., Fu, T., Liu, H., Yao, Y., Zhou, W., et al. (2024). Capacitive low-frequency hydrophone based on micronanostructured iontronic hydrogel for underwater monitoring. *ACS Nano* 18, 22010–22020. doi:10.1021/acsnano.4c04094

Zhou, S. T., Mo, T. F., Ren, X. D., Xu, Q., Sun, Q. Z., Zhang, S. Q., et al. (2024). Experimental study on pulsation and energy characteristics of bubbles produced by underwater electrical explosion. *Acta Phys. Sin.* 73, 245204. doi:10.7498/aps.73.20240720

Zhufeng, L., Xiaofang, L., Na, W., and Qingyang, Z. (2022). Present status and challenges of underwater acoustic target recognition technology: a review. *Front. Phys.* 10, 1044890. doi:10.3389/fphy.2022.1044890